Characterization of a Lysine-Specific Histone Demethylase from *Arabidopsis thaliana*[†]

Valentina Spedaletti,[‡] Fabio Polticelli,[‡] Viviana Capodaglio,[‡] M. Eugenia Schininà,[§] Pasquale Stano,[‡] Rodolfo Federico,[‡] and Paraskevi Tavladoraki*[,‡]

Department of Biology, University Roma Tre, 00146 Rome, Italy, and Department of Biochemical Science and Laboratory of Functional Genomics and Proteomics, University of Rome La Sapienza, 00185 Rome, Italy

Received October 1, 2007; Revised Manuscript Received February 22, 2008

ABSTRACT: *Arabidopsis thaliana* has four genes with close homology to human histone H3 lysine 4 demethylase (HsLSD1), a component of various transcriptional corepressor complexes that often also contain histone deacetylases and the corepressor protein CoREST. All four *Arabidopsis* proteins contain a flavin amine oxidase domain and a SWIRM domain, the latter being present in a number of proteins involved in chromatin regulation. Here, we describe the heterologous expression and biochemical characterization of one of these *Arabidopsis* proteins (AtLSD1) and show that, similarly to HsLSD1, it has demethylase activity toward mono- and dimethylated Lys4 but not dimethylated Lys9 and Lys27 of histone 3. Modeling of the AtLSD1 three-dimensional structure using the HsLSD1 crystal structure as a template revealed a high degree of conservation of the residues building up the active site and some important differences. Among these differences, the most prominent is the lack of the HsLSD1 Tower domain, which has been shown to interact with CoREST and to be indispensable for HsLSD1 demethylase activity. This observation, together with AtLSD1 peculiar surface electrostatic potential distribution, suggests that the molecular partners of AtLSD1 are probably different from those of the human orthologue.

In eukaryotes, the histone N-terminal tails are subjected to multiple covalent modifications, such as acetylation, methylation, phosphorylation, ubiquitination, sumoylation, and ADP-ribosylation (*1*−*3*). These histone modifications act in a combinatorial manner, thus defining a "histone code", to control chromatin state and gene expression (*4*–*6*). Among these modifications, histone lysine acetylation is the best characterized. This modification is generally associated with transcriptional activation and is dynamically regulated by histone acetyltransferases and deacetylases (*4*). Histone methylation mediated by multiple classes of methyl transferases has emerged as another important mechanism which regulates chromatin structure and function (*4, 7, 8*). Five lysine residues on the tails of histones H3 and H4 (H3K4,[1] H3K9, H3K27, H3K36, and H4K20) as well as K79 located within the core of histone H3 have been shown to be target sites for methylation (*6, 9*). Methylation at these sites has been linked to both transcriptional activation and repression, as well as DNA-damage response (*6, 10*), demonstrating a widespread role for histone methylation in various aspects of chromatin biology. Histone lysine residues can be methylated in three different modes, i.e., mono-, di-, or trimethylation. These differentially methylated lysine residues could serve as docking sites for different effector proteins and/or platforms for chromatin modifiers including histone methylases, deacetylases, or remodeling activities, which then could result in potentially diverse functional outcomes (*11*). Arginine residues within the tails of histones H3 (R2, R17, R26) and H4 (R3) can also be methylated, and this generally leads to transcriptional activation (*12*).

Although some histone modifications, such as acetylation, phosphorylation, and ubiquitination, are highly dynamic, histone methylation had been regarded as irreversible. However, the recent discovery of several histone demethylases which can reverse methylation of arginine and lysine residues has altered this view of histone methylation (*11, 13*−*17*). PAD4/PADI4 was the first reported histone arginine demethylase that demethyliminates monomethylarginine to produce citrulline (*13, 14*). Human lysine-specific demethylase 1 (HsLSD1), also known as KIAA0601, has been recently identified as the first histone demethylase that specifically acts on mono- and dimethylated Lys4 of histone H3 (H3K4me1 and H3K4me2, respectively) in a flavin adenine dinucleotide (FAD) dependent oxidative reaction (*15*). More recently, a new family of histone demethylases has been discovered which contains a jumonji C domain capable of removing methyl groups on lysine residues by hydroxylation-based demethylation (*11, 16, 17*).

[†] This work was supported by the University Roma Tre, the Italian Ministry of University and Research (COFIN-PRIN 2005, p.c. 2005052297_002), and the Federated Ateneum of Science and Technology, University of Rome La Sapienza.

* To whom correspondence should be addressed. Tel: +39 06 57336352. Fax: +39 06 57336321. E-mail: tavlador@uniroma3.it.

[‡] University Roma Tre.

[§] University of Rome La Sapienza.

[1] Abbreviations: H3K4, Lys4 of histone 3; HsLSD1, human lysine-specific demethylase 1; H3K4me1, monomethylated H3K4; H3K4me2, dimethylated H3K4; FLC, flowering locus C; FLD, flowering locus D; H3K4me1-S10pho, monomethylated Lys4 and phosphorylated Ser10 of H3; AtLSD1, *Arabidopsis thaliana* lysine-specific demethylase 1; FAD, flavin adenine dinucleotide; ZmPAO, *Zea mays* polyamine oxidase; IPTG, isopropyl β-D-thiogalactoside.

10.1021/bi701969k CCC: $40.75
Published on Web 04/05/2008

HsLSD1 comprises an N-terminal SWIRM domain and a C-terminal flavin domain which displays homology with members of the amine oxidase family (*15*). The HsLSD1-catalyzed reaction regenerates the methyl-free lysine with concomitant release of formaldehyde and H_2O_2. HsLSD1 has been found in association with the corepressor protein CoREST, the histone deacetylases 1 and 2, the PHD-domain-containing protein BHC80, and the HMG-domain-containing protein BRAF35, among others (*18–20*), and recent studies suggest that its specificity and activity can be modulated by its interacting factors (*19–21*). However, the molecular mechanism by which this regulation is achieved still remains unclear. The crystal structure of HsLSD1, determined in free form or in complex with an HsLSD1-stimulatory domain of human CoREST and substrate-like peptide inhibitors, provided the structural framework to explain its catalytic properties and the active role of CoREST in substrate recognition (*22–27*). Furthermore, mutagenesis studies showed that DNA binding by the CoREST domain is crucial for the demethylation of H3K4 within nucleosomes by the HsLSD1−CoREST complex (*24*). Biochemical assays have also shown that HsLSD1 is able to "read and interpret" the histone code discriminating between peptides bearing different covalent modifications (*5, 28*).

In plants, little is known about histone tail modifications in general and about histone methylation/demethylation processes in particular. Available data provide evidence that *Arabidopsis* euchromatin, in general, is enriched in H3K4me2, while heterochromatin is depleted in H3K4me2 but enriched in H3K9me2 (*29, 30*). Furthermore, it has been demonstrated that the acceleration of flowering by prolonged cold, a process called vernalization, causes changes in histone methylation in discrete domains within a negative regulator of flowering, the flowering locus C (FLC), increasing H3K9 and H3K27 dimethylation and decreasing H3K4 dimethylation (*31*). On the other hand, it has been shown that an *Arabidopsis* homologue of HsLSD1, termed flowering locus D (FLD) and shown to interact with a plant-specific C2H2 zinc finger-SET domain protein (*32*), represses the FLC by histone deacetylation (*33*).

In plants, despite the growing information available on histone methylation, the existence of an enzyme which is able to revert histone methylation has not been demonstrated yet. Here, we report the first biochemical characterization of a plant lysine-specific histone demethylase. More specifically, a lysine-specific histone demethylase from *Arabidopsis thaliana* homologous to HsLSD1 was expressed in a bacterial heterologous system, and the catalytic properties of the recombinant enzyme were determined. The three-dimensional structure of this *Arabidopsis* histone demethylase was also modeled using the HsLSD1 crystal structure as a template and analyzed in comparison with the human orthologue.

MATERIALS AND METHODS

Materials. 4-Aminoantipyrine, 3,5-dichloro-2-hydroxybenzenesulfonic acid, and horseradish peroxidase were purchased from Sigma-Aldrich-Fluka. Restriction and DNA-modifying enzymes were purchased from New England Biolabs, Invitrogen, Stratagene, and Promega. The synthetic human histone H3 peptides with specific modifications H3K4me1 (1–21 aa), monomethylated Lys4 and phosphorylated Ser10 (H3K4me1-S10pho) (1–21 aa), H3K4me2 (1–21 aa), H3K9me2 (1–21 aa), and H3K27me2 (21–44 aa) were purchased from Upstate Group Inc. or synthesized by Thermo Scientific. Recombinant HsLSD1 was kindly provided by Prof. Andrea Mattevi and Dr. Claudia Binda (University of Pavia, Italy).

Sequence Analysis and cDNA Acquisition. EST database searches were performed using the basic local alignment search tool (BLAST) (*34*). Multiple sequence alignment of the amino acid sequences was done using the program CLUSTAL W (*35*). The cDNA encoding for the putative *A. thaliana* histone demethylase (*AtLSD1*; At1g62830; GenBank accession number NM_104961) was obtained from the DNA Stock Center of the *Arabidopsis* Biological Resource Centre (U21563 clone) and completely sequenced to exclude sequence changes compared to the corresponding *A. thaliana* genomic sequence.

Expression of Recombinant AtLSD1 in Escherichia coli. The pET17b vector (Novagen) was used to construct an *AtLSD1* prokaryotic expression system. To clone *AtLSD1* cDNA between restriction sites *Xba*I and *Xho*I of this vector, the whole coding region of the *AtLSD1* cDNA was amplified using the U21563 clone (*Arabidopsis* Biological Resource Center) as a template and the sequence-specific oligonucleotides *AtLSD1for1* (5′-GTCTAGAAATAATTTTGTTTAACTTTAAGAAGGAGATATACATATGTCAACAGAGACTAAAGAAACCCGACCC-3′)/*AtLSD1rev1* (5′-GCTCGAGCTAGTGGTGGTGGTGGTGGTGTCCTCCATCAAAGATCTGTCGATTCAGTC TTGCAGC-3′). The underlined regions in *AtLSD1for1* and *AtLSD1rev1* oligonucleotides indicate *Xba*I and *Xho*I restriction sites, respectively. The *AtLSD1rev1* primer was designed to insert the coding sequence for two Gly residues and a 6-His tag prior to the stop codon of the *AtLSD1* cDNA. The amplified *AtLSD1* cDNA was subcloned into the pDrive vector (Qiagen), completely sequenced, and then cloned in the pET17b plasmid yielding the construct *AtLSD1*-pET17b. This plasmid was then used to transform *E. coli* BL21 (DE3) cells. Expression of recombinant AtLSD1 was induced by 0.4 mM isopropyl β-D-thiogalactoside (IPTG) at 25 °C for 5 h. Cells were resuspended in extraction buffer [50 mM Tris-HCl, pH 8.0, 0.1 M NaCl, 10% (v/v) glycerol, 1 mM phenylmethanesulfonyl fluoride] and disrupted by sonication. After centrifugation at 13000*g* for 30 min at 4 °C, the clear supernatant (bacterial extract) containing the soluble proteins was either analyzed for recombinant protein accumulation by immunoblotting or further processed for recombinant protein purification.

Purification of Recombinant AtLSD1 from Bacterial Extracts. Recombinant AtLSD1 was purified from bacterial extracts by affinity chromatography. In detail, bacterial extracts were applied to a Ni^{2+}-charged resin (Amersham Biosciences) equilibrated in extraction buffer. The resin was washed first with extraction buffer and then with 50 mM Tris-HCl, pH 8.0, 50 mM NaCl, and 10% (v/v) glycerol. The protein was eluted with 50 mM Tris-HCl, pH 8.0, 50 mM NaCl, 10% (v/v) glycerol, and 100 mM imidazole. The fractions enriched in recombinant AtLSD1 were pooled, diluted 5-fold with 50 mM Tris-HCl, pH 8.0, and 10% (v/v) glycerol, and chromatographed on a HiTrap heparin HP column (Amersham Biosciences) equilibrated in 50 mM Tris-HCl, pH 8.0, 10 mM NaCl, and 10% (v/v) glycerol. Elution was performed with a nonlinear gradient of NaCl (50 mM−2

M) in Tris-HCl, pH 8.0, and 10% (v/v) glycerol. AtLSD1-containing fractions (fractions of 200 or 400 mM NaCl) were dialyzed against 50 mM Tris-HCl, pH 8.0, and 10% (v/v) glycerol and concentrated using centrifugal filter devices (Millipore). Recombinant protein was quantified by absorption spectroscopy using an extinction coefficient of 10790 M^{-1} cm^{-1} at 458 nm (*36*) and stored at 4 °C. The purity of the recombinant enzyme was determined by SDS−PAGE analysis and by the ratio A_{280}/A_{458}, which was about 10. Using this two-step purification protocol, a yield of 1 mg/L of culture has been obtained.

CD Spectroscopy. CD spectra were recorded at 25 °C using a Jasco J-600 spectropolarimeter and quartz cells having 0.05 cm path length. Recombinant AtLSD1 was at a concentration of 0.3 mg/mL in 15 mM Tris-HCl and 3% (v/v) glycerol, pH 8.0. Instrumental ellipticity was converted into mean residue molar ellipticity [θ] (deg cm^2 $dmol^{-1}$) after spectrophotometric determination of the protein concentration. For each sample, nine CD spectra in the far-UV region (198–250 nm) were recorded and averaged. Secondary structures were estimated by using CONTIN, K2D, and SELCON3 algorithms provided by the free software Dicroprot2000 (*37*).

Determination of AtLSD1 and HsLSD1 Catalytic Parameters. The catalytic parameters (K_m and k_{cat}) of recombinant AtLSD1 and HsLSD1 were determined using about 2.0 μM purified protein in a 300 μL reaction volume by following spectrophotometrically the formation of a pink adduct ($\epsilon_{515} = 2.6 \times 10^4$ M^{-1} cm^{-1}), as a result of oxidation of 4-aminoantipyrine and 3,5-dichloro-2-hydroxybenzenesulfonic acid catalyzed by horseradish peroxidase in 50 mM Tris-HCl and 30% glycerol, pH 8.0 (except as otherwise indicated) at 25 °C (*5, 36, 38*). k_{cat} values were calculated using saturating concentrations of methylated H3K4 peptides (147 μM) and keeping the O_2 concentration constant at the air-saturated level (apparent k_{cat}). K_m values were determined from Michaelis–Menten plots using variable concentrations of peptides (2–147 μM) and a constant O_2 concentration at the air-saturated level (apparent K_m).

Demethylation Assay by Western Blot Analysis. H3K4met2 peptide (0.29 mM) was incubated with purified recombinant AtLSD1 (0.02 mM) in 50 mM Tris-HCl, pH 8.0, and 30% (v/v) glycerol for 2 h at room temperature. The demethylase activity of AtLSD1 was evaluated by Western blot analysis using an anti-H3K4met2 (Upstate Group Inc.) methylation-specific antibody.

Demethylation Assay by Matrix-Assisted Laser Desorption/Ionization (MALDI) Mass Spectrometry. H3K4me1, H3K4me2, H3K9me2, and H3K27me2 peptides at a concentration of 0.2 mM were incubated with purified recombinant AtLSD1 (0.02 mM) in 50 mM Tris-HC, pH 8.0, and 10% (v/v) glycerol for 4 h at room temperature. An aliquot of each sample (1 μL) was mixed with the α-cyano-4-hydroxy-*trans*-cinnamic acid matrix solution (10 mg/mL in 70% acetonitrile containing 0.2% trifluoroacetic acid) in different ratios (1:3, 1:5, 1:10); 1 μL of each mixture was deposited onto a MALDI target plate and allowed to dry on air. MALDI-TOF MS analyses were performed in a Voyager-DE STR instrument (Applied Biosystems, Framingham, MA) equipped with a 337 nm nitrogen laser and operating in reflector mode. Mass data were obtained by accumulating spectra from 200 laser shots with an accelerating voltage of 20 kV. All mass spectra were externally calibrated using a standard peptide mixture (Sequizyme; Applied Biosystems).

SDS−PAGE and Western Blot Analysis. SDS−PAGE was carried out according to the method of Laemmli (*39*). Recombinant AtLSD1 from bacterial extracts was subjected to SDS−PAGE (10% polyacrylamide) and analyzed either by staining with Coomassie Brilliant Blue or by Western blot using a mouse anti-6-His monoclonal antibody (Sigma-Aldrich-Fluka) and a rabbit anti-mouse antibody coupled to horseradish peroxidase (Amersham Biosciences). In the latter case, proteins were transferred to a nitrocellulose membrane (Schleicher & Schuell) using a Mini Trans-Blot apparatus (Bio-Rad), following the manufacturers' instructions. For Western blot analysis of the H3K4me2 peptide, proteins were separated by SDS−PAGE (15% polyacrylamide), electrophoretically transferred to a polyvinylidene difluoride (PVDF) membrane (Immobilon PSQ; Millipore) at 150 mA for 45 min, and incubated first with a rabbit anti-H3K4me2 methylation-specific antibody (Upstate Group Inc.) and then with a goat anti-rabbit antibody coupled to horseradish peroxidase (Vector Laboratories, Inc.). The detection of the labeled proteins was done with a chemiluminescence kit (Boehringer-Mannheim).

DNA Sequencing. DNA sequencing was performed on double-stranded plasmid DNA using the automated fluorescent dye terminator technique (Perkin-Elmer ABI model 373A).

Semiquantitative RT-PCR Analysis of Lysine-Specific Histone Demethylase Genes in Various Arabidopsis Organs. Total RNA was isolated from various plant organs (rosette leaves, cauline leaves, stems, inflorescences, silique, and roots) of *A. thaliana* (ecotype Columbia) plants using TRIZOL reagent (Invitrogen) and/or the RNeasy Mini kit (Qiagen) according to the manufacturers' instructions. To extract total RNA from the silique, a method modified from the RNeasy Mini kit was used (*40*). RNA samples were treated with RNase-free DNase I (Invitrogen) to avoid amplification from genomic DNA. The first cDNA strand was synthesized from total RNA using the SuperScript III first-strand synthesis system for RT-PCR (Invitrogen) and random primers. Aliquots of reverse-transcribed RNA were amplified by 25, 28, 30, 35, or 40 PCR cycles (denaturation at 94 °C for 1 min, annealing at 58 °C for 30 s, and extension at 72 °C for 1 min) using gene-specific primers. The *AtLSD1*-specific primers were *AtLSD1for2* (5-CAACAGAGACTAAAGAAACCCGACC-3′) and *AtLSD1rev2* (5′-CGGCGGTTTCTTGAGAAAGCTGGG-3′); the *AtLSD2*-specific primers were *AtLSD2for* (5′-CCGAGGAGGAACAGGAGAAAAGTAAG-3′) and *AtLSD2rev* (5′-AGTACCCTCTTCAGGAATATAAGGAGCAA); the *AtLSD3*-specific primers were *AtLSD3for* (5′-GCACCAAAGAAACGAAGGAGAGGACG-3′) and *AtLSD3rev* (5′-GCCGAATCTAAGAGACTACTACAATGTTTAGGAATC-3′); the *AtLSD4*-specific primers were *AtLSD4for* (5′-CAGCGCCAGGGTTTTTCTGTAACC-3′) and *AtLSD4rev* (5′-TCTCAGCCGTTGAAGGCCATATTCT-3′). PCR amplification was carried out with the BIOTAQ DNA polymerase (Bioline) in an iCycler thermal cycler (Bio-Rad). To confirm equal amounts of RNA among the various samples, UBQ5 expression was used using the gene-specific primers *UBQ5for* (5′-GGAAGAAGAAGACTTACACC-3′) and *UBQ5rev* (5′-AGTCCACACTTACCACAGTA-3′). Results at the exponential phase (usually

at 28 cycles for *AtLSD1*, *AtLSD2*, and *AtLSD3*, at 30 cycles for *AtLSD4*, and at 25 cycles for *UBQ5*) were analyzed.

Molecular Modeling and Structure Analysis. The three-dimensional structure of AtLSD1 was homology modeled using the structure of HsLSD1 as a template [PDB code 2IW5 (*24*)]. In detail, a PSI-BLAST (*34*) search on the nonredundant sequence database was carried out to retrieve amino acid sequences displaying significant similarity to AtLSD1. The best 18 sequences, which included the template HsLSD1 sequence, were then subjected to a multiple alignment procedure using CLUSTAL W (*35*). From the multiple alignment obtained with this procedure a pairwise alignment between AtLSD1 and HsLSD1 was extracted and used for the homology modeling procedure. The AtLSD1 model was then built using the program NEST, a software to build protein models based on a given alignment between query sequence and template which uses an artificial evolution method (*41*). The NEST option *−tune 2* was used to refine the alignment, avoiding the unlikely occurrence of insertions and deletions within template secondary structure elements. The quality of the final AtLSD1 model was then probed using the program PROCHECK (*42*). The overall *G*-value of the model resulted in being –0.22, well above the PROCHECK threshold of –0.5 for good quality models. The complex between AtLSD1 and a substrate-like peptide inhibitor was modeled by superimposition of the three-dimensional model of AtLSD1 with the three-dimensional structure of the complex formed by HsLSD1 with the peptide inhibitor [PDB code 2V1D (*26*)]. Surface electrostatic potential of AtLSD1 and HsLSD1 was calculated using the DelPhi program (*43*) and visualized using Chimera (*44*). In detail, hydrogen atoms were added to the structures using the routine HBUILD of the CHARMM package (*45*) and the CHARMM27 parameters and force field (*46*). Structures were then stereochemically regularized by energy minimization, applying a harmonic force of 10 kcal/mol to non-hydrogen atoms. In the DelPhi calculations, values of 2 and 80 were used for the dielectric constant of the protein interior and solvent, respectively. The ionic strength value was set to 0.05 M.

RESULTS

Description of a Lysine-Specific Histone Demethylase Gene Family in A. thaliana. A search of the *A. thaliana* genome database using the amino acid sequence of *Zea mays* polyamine oxidase (ZmPAO) revealed the presence of five cDNAs encoding for putative PAOs (*47*), plus four additional ones (*At1g62830*, *At3g13682*, *At3g10390*, *At4g16310*) coding for proteins bearing a flavin amine oxidase domain signature together with a SWIRM domain (Figure 1) (*15, 32*). The latter proteins display 26−30% sequence homology with HsLSD1, which is also known to possess both a flavin amine oxidase domain and a SWIRM domain and which specifically demethylates histone H3K4me1 and H3K4me2 (*5, 15*). Thus, it was hypothesized that these four *A. thaliana* cDNAs also encode for lysine-specific histone demethylases, and they were termed *AtLSD1* (*A. thaliana* lysine-specific demethylase 1), *AtLSD2*, *AtLSD3*, and *AtLSD4*, respectively. Interestingly, despite the high sequence homology with HsLSD1, the amino acid sequence homology of the four AtLSDs with the two yeast demethylases [SWIRM1 and SWIRM2 (*48*)], for which, however, histone demethylase activity has not yet been demonstrated, is very low (11–18%). AtLSD1, AtLSD2, and AtLSD3 display a fairly high overall sequence homology with each other (48–52%) and with AtLSD4 (25%–30%), which extends to both the amine oxidase and the SWIRM domains (Figure 1B).

To determine the possible subcellular localization of the four putative *Arabidopsis* histone demethylases, the amino acid sequences were analyzed using PSORT (www.psort.ims.u-tokio.ac.jp). This analysis predicted the presence of a nuclear localization signal at positions 517–534 of the AtLSD1 amino acid sequence, suggesting sorting to the nucleus similarly to HsLSD1 (*49*). This has been recently confirmed by transient expression studies of AtLSD1 tagged with green fluorescent protein (*32*). Nuclear localization was predicted also for AtLSD2 and AtLSD4, while mitochondrial/chloroplastic localization was predicted for AtLSD3. Furthermore, analysis of the amino acid sequence of the four AtLSDs for the presence of specific sequence motifs did not evidence the presence of HMG DNA-binding domains, as has been shown for the two yeast demethylases (*48*).

The expression pattern of the *AtLSD* gene family in different *Arabidopsis* organs (rosette and cauline leaves, stem, flowers, roots, and siliques) was also analyzed by semiquantitative RT-PCR using gene-specific primers (Figure 2). This analysis showed that the AtLSD1 transcript is present at similar levels in all tested organs, even though expression levels were expected to be higher in the flowers than in the other tissues considering the proposed role of chromatin remodeling enzymes in flowering control (*50*). Similar results were obtained also for AtLSD2, AtLSD3, and AtLSD4 transcripts (Figure 2). These data are in agreement with microarray data obtained from the *A. thaliana* database (Genevestigator expression analysis), which, however, demonstrate the differential expression pattern in specific parts or at specific developmental stages of the various organs, as, for example, in the shoot apex during transition from the vegetative to the inflorescence state.

Heterologous Expression and Biochemical Characterization of AtLSD1 in E. coli. To verify whether the *AtLSD* gene family encodes for proteins with a lysine-specific histone demethylase activity, heterologous expression of AtLSD1, chosen as representative member of the family, in *E. coli* was attempted using the pET17b vector which guides cytoplasmic expression of recombinant proteins. To facilitate purification of the recombinant protein, a sequence encoding for a 6-His tag was added at the 3′ terminus of the *AtLSD1* cDNA in the *AtLSD1*-pET17b plasmid. Western blot analysis using an anti-6-His tag antibody of bacteria transformed with *AtLSD1*-pET17b plasmid and treated with IPTG confirmed recombinant AtLSD1 accumulation in the soluble bacterial extracts (data not shown).

To purify the recombinant AtLSD1, affinity chromatography on a resin charged with Ni^{2+} was performed, which, however, was not sufficient to purify the recombinant protein to electrophoretic homogeneity (Figure 3). Thus, the pooled elution fractions from the Ni^{2+} resin were further chromatographed on a HiTrap heparin HP column from which the protein was recovered at a homogeneity greater than 95% (Figure 3). The purified protein displayed the characteristic

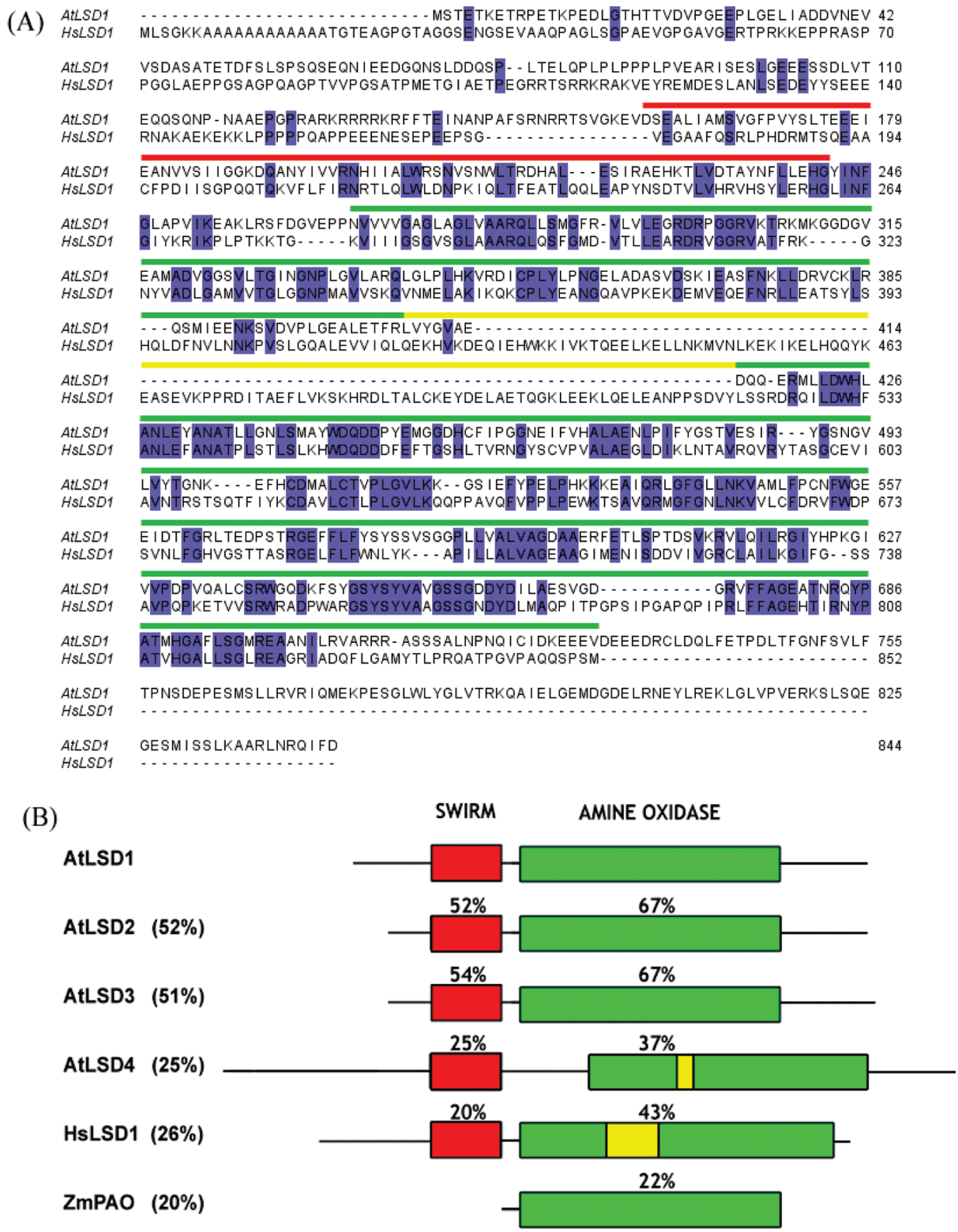

FIGURE 1: AtLSDs, HsLSD1, and ZmPAO sequence comparison. (A) Amino acid sequence alignment of AtLSD1 and HsLSD1. Strictly conserved residues are indicated by blue boxes. Red lines above the alignment indicate the SWIRM domain, green lines indicate the amine oxidase domain, and yellow lines indicate the Tower domain. (B) Schematic representation of the various domains of AtLSD1 (At1g62830; GenBank accession number NM_104961), AtLSD2 (At3g13682; GenBank accession number NM_112218), AtLSD3 (At3g10390; FLD; GenBank accession number NM_111874), AtLSD4 (*At4g16310*; GenBank accession number NM_117726), HsLSD1 (GenBank accession number NM_015013), and ZmPAO (GenBank accession number AJ002204). Red boxes indicate the SWIRM domains, green boxes indicate the amine oxidase domains, and yellow boxes the Tower domain. Numbers indicate the percentage of amino acid sequence homology, as a whole or by domain, of the various proteins with respect to AtLSD1.

UV–visible spectrum of the oxidized flavoproteins with three absorbance peaks at 280, 380, and 460 nm (data not shown) and an apparent molecular mass of 94 kDa (Figure 3), the molecular mass expected for the recombinant protein from amino acid sequence analysis. Precipitation of purified AtLSD1 with trichloroacetic acid resulted in the release of

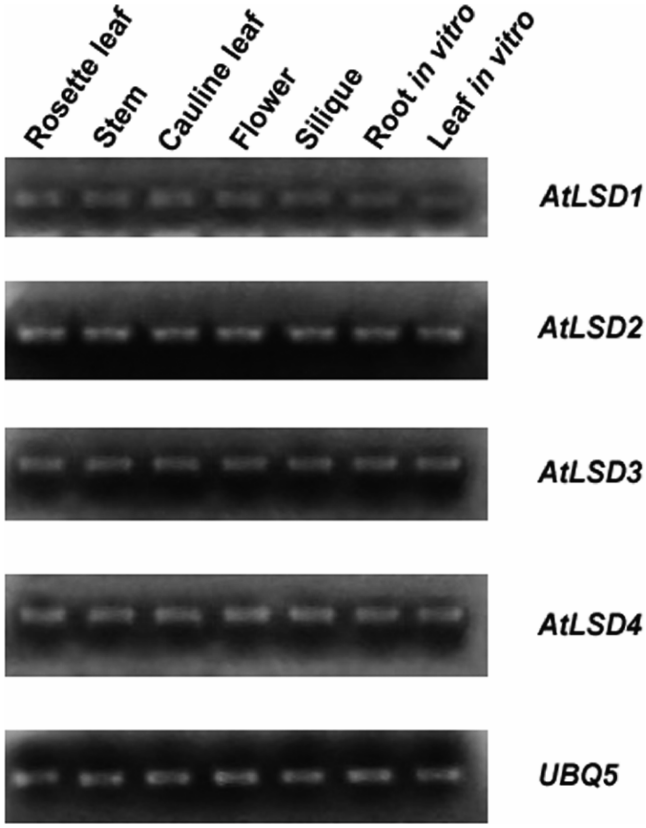

FIGURE 2: Expression pattern of *AtLSD1*, *AtLSD2*, *AtLSD3*, and *AtLSD4* in various *Arabidopsis* organs. The expression of the four *AtLSD* genes in various *Arabidopsis* organs (rosette and cauline leaves, stems, flowers, roots, and siliques) was analyzed by semi-quantitative RT-PCR using gene-specific primers. *UBQ5* expression was used to confirm an equal amount of RNA among the various samples. Results at the exponential phase (at 28 cycles for *AtLSD1*, *AtLSD2*, and *AtLSD3*, at 30 cycles for *AtLSD4*, and at 25 cycles for *UBQ5*) are shown.

the cofactor into the supernatant, indicating noncovalent binding to the protein.

Purified recombinant AtLSD1 was tested for its ability to oxidize various methylated H3 peptides and various polyamines using a peroxidase-coupled assay to quantify H_2O_2 levels (*5, 36, 38*). The results evidenced that, similarly to HsLSD1, the recombinant enzyme is able to demethylate H3K4me2 and H3K4me1 peptides, the specific activity with the H3K4me2 peptide being higher than that with the H3K4me1 peptide (Table 1). Furthermore, the results also showed that AtLSD1 is not able to oxidize either the H3K9me2 and H3K27me2 peptides or the common polyamines spermine, spermidine, and putrescine. The ability of recombinant AtLSD1 to demethylate the H3K4me2 peptide was also analyzed by a Western blot based assay using an anti-H3K4me2 methylation-specific antibody to detect the dimethylation status of the peptide (*15*). This analysis confirmed that the recombinant protein efficiently reduces the dimethylation level of the H3K4me2 peptide (Figure 4). Demethylase activity of AtLSD1 was further confirmed by mass spectrometry analysis. Demethylation of the H3K4me1 and H3K4me2 peptides by AtLSD1 is expected to regenerate the unmodified peptide with the net loss of 14 and 28 Da, respectively, corresponding to the molecular mass of one or two CH_2 group(s). The H3K4me1, H3K4me2, H3K9me2, and H3K27me2 peptides were incubated with purified recombinant AtLSD1 or buffer, and the reaction mixtures were analyzed by mass spectrometry. In the absence of AtLSD1, the H3K4me1 and H3K4me2 peptides display molecular masses of 2268 and 2282, respectively, as expected for these

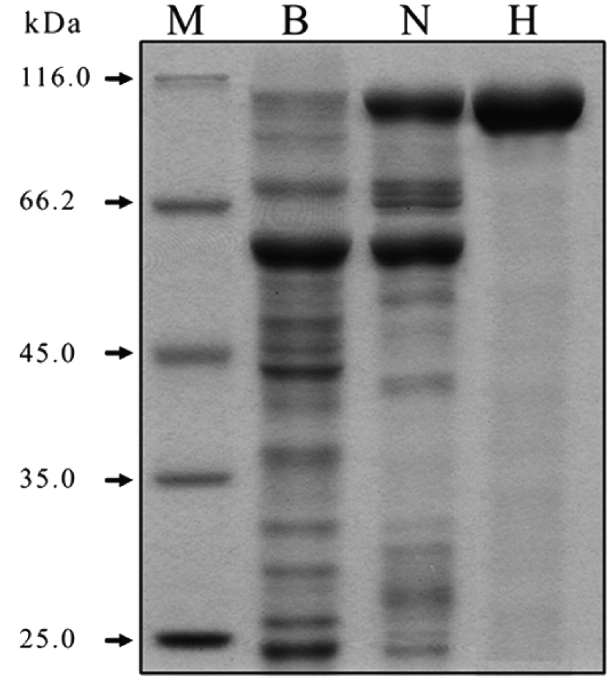

FIGURE 3: Purification of recombinant AtLSD1 expressed in bacteria. Analysis of representative protein samples from each stage of the purification protocol by SDS−PAGE (10% polyacrylamide). Key: B, crude bacterial extract; N, pooled elution fractions from the Ni^{2+}-charged resin; H, pooled elution fractions from the HiTrap heparin HP column; M, molecular mass marker.

Table 1: Kinetic Constants for the Demethylation of H3 Peptides by Recombinant AtLSD1 and HsLSD1

peptide	k_{cat} (min^{-1})[a]	K_m (μM)[a]
AtLSD1		
H3K4me1	0.50 ± 0.06	8.9 ± 0.8
H3K4me2	0.68 ± 0.08	10.7 ± 0.6
H3K4me2 in 10% glycerol[b]	0.34 ± 0.08	12.8 ± 1.0
H3K4me1-S10pho	no activity	no activity
HsLSD1−CoREST		
H3K4me1	6.50 ± 0.60	6.1 ± 0.6

[a] Enzymatic activity of recombinant AtLSD1 and of recombinant HsLSD1 in complex with CoREST (HsLSD1−CoREST) was determined in 50 mM Tris-HCl and 30% glycerol, pH 8.0, using a constant O_2 concentration at the air-saturated level and a peptide concentration either saturating (147 μM for apparent k_{cat} determination) or varying between 2 and 147 μM (for apparent K_m determination). Data are the mean ± SEM of at least three independent experiments. [b] The assay was performed in 50 mM Tris-HCl and 10% glycerol, pH 8.0. Similar results were obtained in the absence of glycerol.

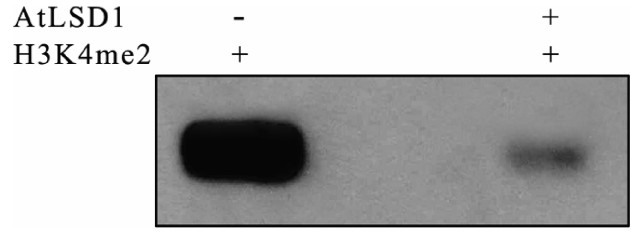

FIGURE 4: Demethylation of H3K4me2 peptide by recombinant AtLSD1. H3K4me2 peptide was incubated for 2 h with recombinant AtLSD1 and analyzed by Western blot using an anti-H3K4me2 methylation-specific antibody.

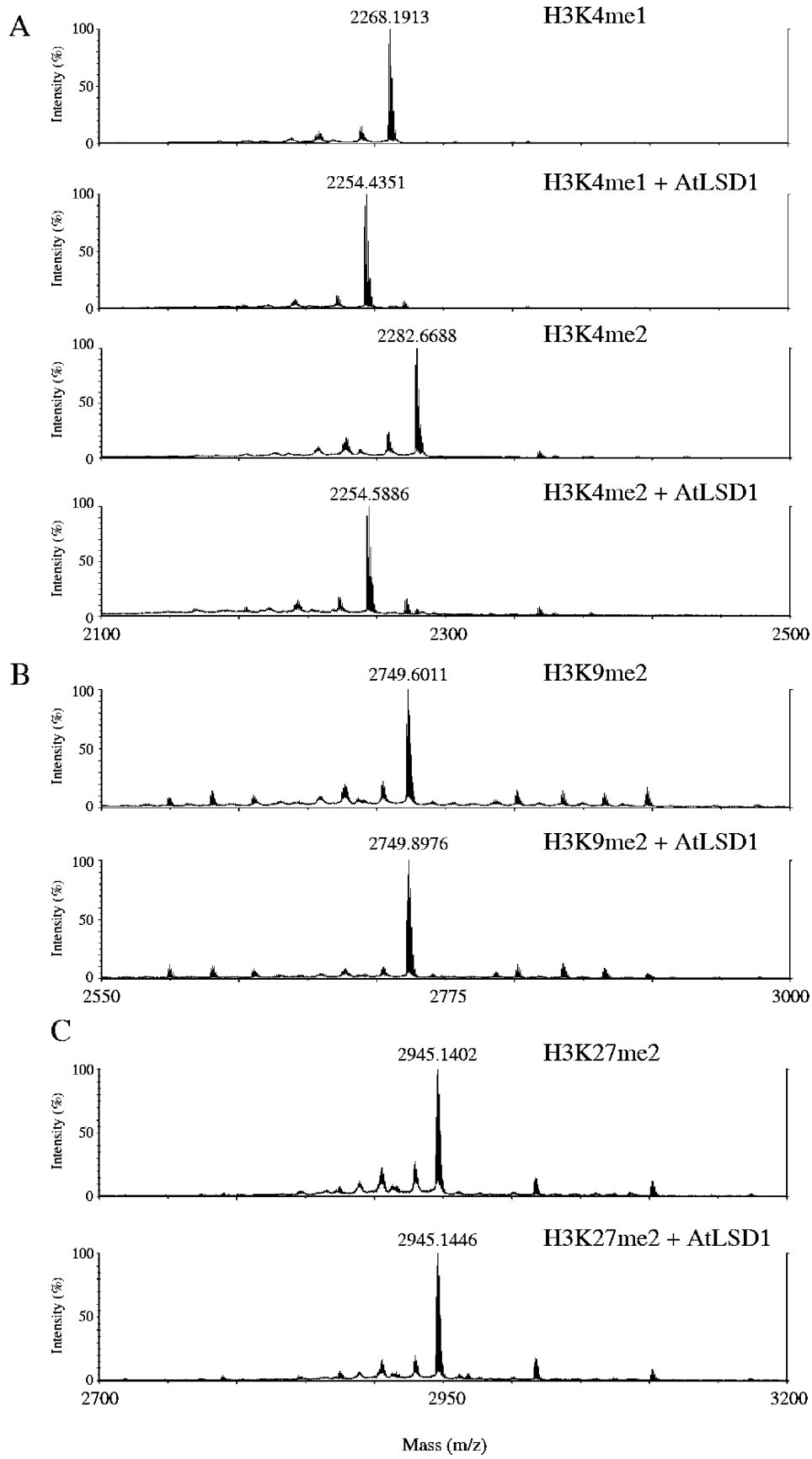

FIGURE 5: Mass spectrometry analysis of methylated H3 peptides after incubation with recombinant AtLSD1. H3K4me1 and H3K4me2 (panel A), H3K9me2 (panel B), and H3K27me2 (panel C) peptides were incubated for 4 h with buffer or purified recombinant AtLSD1, and reaction mixtures were analysed by mass spectrometry.

peptides (Figure 5, panel A). In the presence of AtLSD1 for both peptides a new peak appeared at a molecular mass of 2254, which well corresponds to the molecular mass of the demethylated peptide (Figure 5, panel A). On the contrary,

the peaks corresponding to the H3K9me2 and H3K27me2 peptides were found to be unaffected by incubation with recombinant AtLSD1 (Figure 5, panels B and C).

The activity of the recombinant enzyme with the H3K4me2 and H3K4me1 peptides was shown to be higher at pH 8.0 than at pH 6.0 or at pH 9.0 (data not shown) and to increase at higher glycerol concentrations (50% increase in the presence of 30% glycerol as compared to that in the presence of 0–10% glycerol) (Table 1). Interestingly, k_{cat} values of AtLSD1 were shown to be about 10-fold lower than that of HsLSD1 in free form (*5*) or in complex with CoREST (present study and ref *26*) (Table 1). Misfolding of the recombinant protein can be excluded on the basis of CD spectroscopy analysis, which indicated a high secondary structure content, the α-helix/β sheet percentage being 38−44% as calculated using CONTIN (*51*), K2D (*52*), or SELCON3 (*53*) methods. AtLSD1 catalytic activity resulted strongly inhibited in the presence of 50 mM KCl (50% inhibition) or $MgCl_2$ (75% inhibition), which suggests that electrostatic interactions are an important factor in AtLSD1 catalytic activity, as has been also demonstrated for HsLSD1 (*5*). Furthermore, phosphorylation of the H3Ser10 residue totally abolished the AtLSD1 demethylase activity toward the H3K4me1 peptide, as shown by the lack of any detectable activity of recombinant AtLSD1 toward the H3K4me1-Ser10pho peptide (Table 1).

Comparative Analysis of the Three-Dimensional Structure of AtLSD1. Figure 6 shows the three-dimensional structure of AtLSD1 modeled using the HsLSD1 crystal structure as a template [PDB code 2IW5 (*24*)]. As already predicted on the basis of the amino acid sequence alignment (Figure 1), the most striking difference between the two proteins is the almost complete absence of the Tower domain in AtLSD1. On the other hand, comparative analysis of the active site structures of AtLSD1 and HsLSD1 reveals a high degree of conservation of the residues building up the site, major substitutions in AtLSD1 being only Ser for Met332, Tyr for Trp695, and Tyr for Phe538 (Figure 7). However, none of these residues are involved in direct contacts with the substrate-like pLys4Met peptide inhibitor in HsLSD1 (*26*). In addition, modeling of the complex formed between AtLSD1 and this substrate-like peptide inhibitor, modeled by superimposition of the three-dimensional model of AtLSD1 with the three-dimensional structure of the complex formed by HsLSD1 with the peptide inhibitor [PDB code 2V1D (*26*)], highlights the strict conservation of the complex network of interactions observed between the peptide inhibitor and HsLSD1 (Figure 7). In particular, the acidic patch formed by Asp375, Glu379, and the carbonyl group of Cys360, which in HsLSD1 interacts with the peptide pArg8 residue, is strictly conserved in AtLSD1 (residues Asp367, Glu371, and Cys352). Strict conservation is also observed for residues Asp553 and Asp556 of HsLSD1 which bind the peptide pArg2 residue (Asp446 and Asp449 of AtLSD1). In addition, several hydrogen bonds which stabilize the HsLSD1 complex with the substrate-like peptide inhibitor are also conserved in the modeled AtLSD1 complex: (1) the hydrogen bond between Asn383 (Asn375 in AtLSD1) and the backbone nitrogen atoms of pThr11 and pGly12; (2) the hydrogen bond between His564 (His457 in AtLSD1) and the Oγ atom of pThr6; (3) the hydrogen bonds between the backbone nitrogen of pAla1 and Asn540 side-chain carbonyl group and Ala539 backbone carbonyl group (Asn433 and Ala432 in AtLSD1). Finally, it is also conserved in the HsLSD1 Tyr761 residue (Tyr650 in AtLSD1) which interacts with the pMet4 residue of the substrate-like inhibitor, the latter residue mimicking the dimethylated Lys4 of the histone H3 tail (Figure 7) (*26*).

Analysis of the surface electrostatic potential of AtLSD1 as compared to that of HsLSD1 evidenced a higher negative character of both the active site region and the SWIRM domain (Figure 6). This feature, together with the absence of the HsLSD1 Tower domain, is probably related to the interaction of AtLSD1 with different molecular partners. As a matter of fact, a BLAST search using human CoREST as a bait did not retrieve any protein in the *A. thaliana* genome displaying significant similarity with CoREST.

DISCUSSION

In the present study it was demonstrated that AtLSD1 is a lysine-specific histone demethylase with a substrate specificity similar to that of HsLSD1. In particular, recombinant AtLSD1 is able to specifically demethylate H3K4me2 and H3K4me1 peptides, whereas it shows no activity toward H3K9me2 and H3K27me2 peptides and polyamines. Data presented in this paper represent the first demonstration that also in plants histone methylation is a reversible process. This is an important finding considering that in plants histone modifications are involved in key developmental processes, such as the transition from the vegetative to the reproductive stage (*50*), and will probably contribute to get a better understanding of the underlying mechanism(s). In a recently published study (*32*), the authors failed to detect demethylase activity of their recombinant AtLSD1. In the light of the results described in this paper, it must be concluded that this may be due to instability and/or incorrect folding of the recombinant protein under their experimental conditions. Indeed, we have observed that AtLSD1 catalytic activity resulted greatly enhanced in the presence of increasing amounts of glycerol.

A comparative analysis of the AtLSD1 and the HsLSD1 amino acid sequence and three-dimensional structure showed a high degree of conservation of the residues building up the active site and interacting with the pLys4Met peptide inhibitor. This is in line with the observation that the ionic strength influences the catalytic activity of both the human and the plant enzymes, which suggests that electrostatic interactions are an important factor in the catalytic activity of both enzymes. Similarly, phosphorylation of the H3Ser10 residue, another important epigenetic mark, totally abolishes the demethylase activity toward the H3K4me1 peptide of both AtLSD1 and HsLSD1, probably due to unfavorable electrostatic interactions which make the peptide unable to bind the enzymes in a productive way (*5*). These data suggest that, similarly to the human demethylase, AtLSD1 is able to "read" different epigenetic marks on the histone N-terminal tail, a finding which may have an important biological significance.

A prominent difference between AtLSD1 and HsLSD1 is the lack of the HsLSD1 Tower domain in the AtLSD1. This domain has been shown to be crucial for the histone demethylase activity of HsLSD1 (*22, 23*) and to be involved in HsLSD1−CoREST complex formation (*23, 24*), which

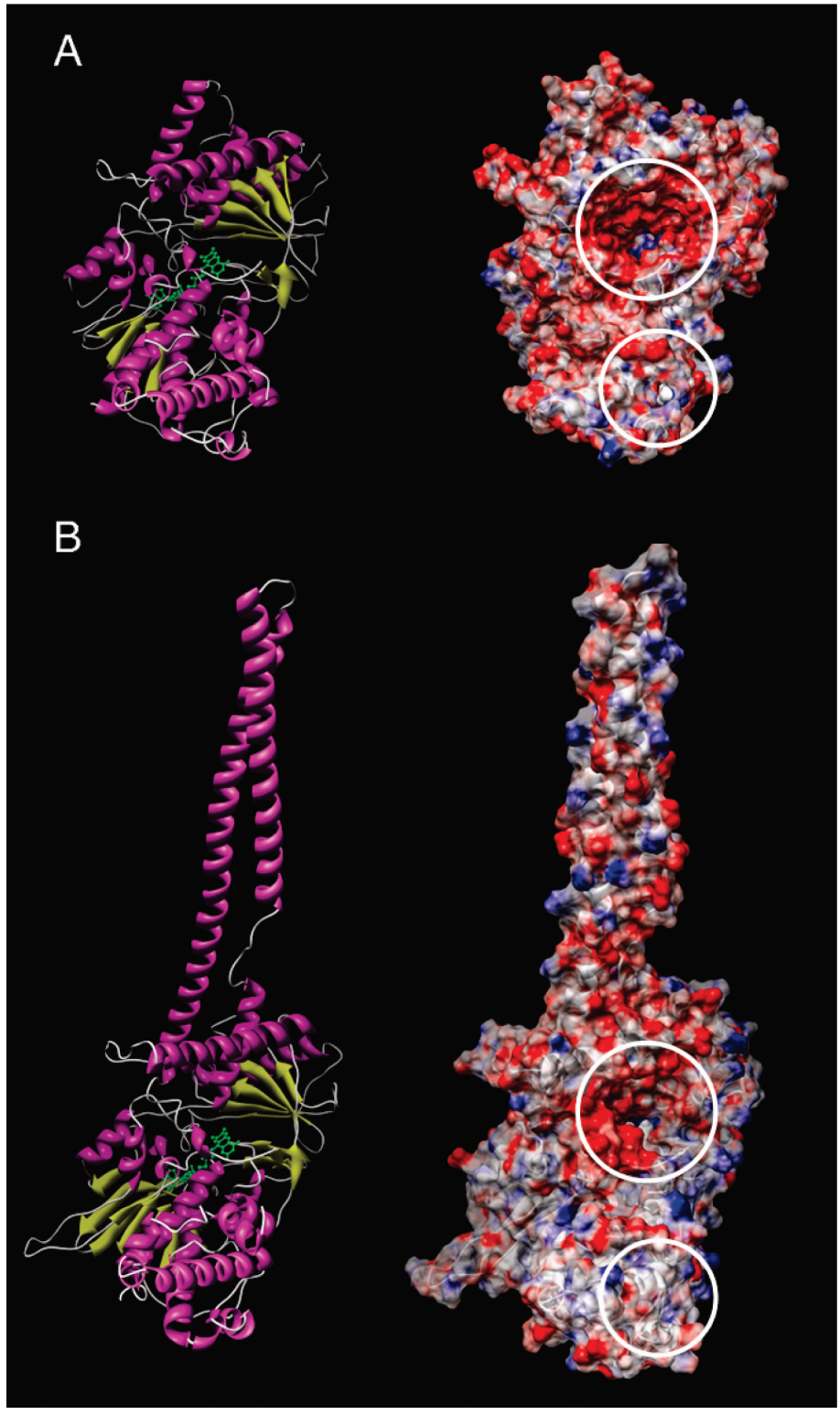

FIGURE 6: Schematic representation of the modeled three-dimensional structure of AtLSD1 (A) and of the crystal structure of HsLSD1 [PDB code 2IW5 (*24*)] (B). The FAD cofactor is shown in green to identify the active site region. Surface electrostatic potential contoured at +10 kT/e (blue) and –10 kT/e (red) is shown on the right panel. White circles highlight differences in the surface electrostatic potential between the two proteins.

in turn has been shown to stimulate the demethylase activity of HsLSD1 toward nucleosomes (*19, 20*). In the case of AtLSD1, despite the lack of the Tower domain, a lysine-specific histone demethylase activity has been demonstrated. However, AtLSD1 and HsLSD1 differ significantly from each other in catalytic efficiency. In particular, AtLSD1 displays a turnover rate 10-fold lower than that of HsLSD1. From this viewpoint it must be noted that a Towerless mutant of HsLSD1 has been shown to have a greatly reduced catalytic activity (approximately 0–10% as compared to the wild-type enzyme) (*22, 23*), indicating that the Tower domain may be involved in the structural organization of the active site. These data suggest that small structural differences in the active site of AtLSD1 due to the lack of the Tower

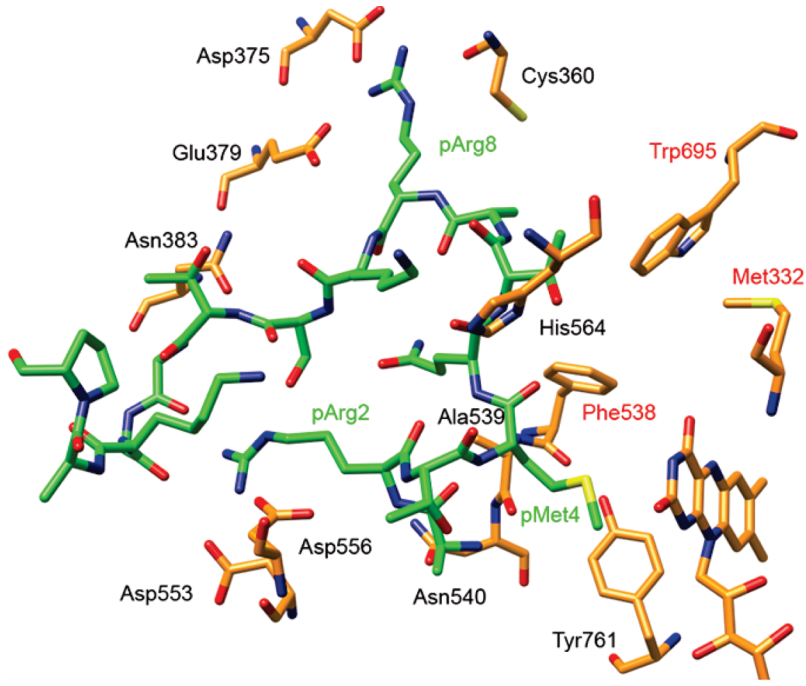

FIGURE 7: Schematic view of the complex formed by HsLSD1 with the substrate-like pLys4Met peptide inhibitor [PDB code 2V1D (*26*)]. HsLSD1 and peptide inhibitor residues contributing to the complex formation (see text) are labeled in black and green, respectively. For reasons of clarity, carbon atoms of HsLSD1 are colored in orange and those of the peptide inhibitor in green. Active site HsLSD1 residues nonconserved in AtLSD1 (substitutions being Met332Ser, Phe538Tyr, and Trp695Tyr) are labeled in red. Note that none of the nonconserved residues interacts with the peptide inhibitor in the HsLSD1 complex.

domain could explain the lower efficiency of this enzyme in respect to the human orthologue. However, it is also possible that AtLSD1 interacts *in vivo* with other proteins, as some recent data indicate (*32*), which may affect its catalytic properties and increase its efficiency. Functional partners of AtLSD1 seem to be different from those of HsLSD1. This is supported not only by the absence in the former protein of the Tower domain but also by a peculiar electrostatic potential distribution of the SWIRM molecular surface. In addition, the sequence similarity search using CoREST as a bait does not retrieve any protein in the *A. thaliana* genome which displays a significant sequence similarity with CoREST, ruling out the possibility that AtLSD1 interacts with CoREST-like macromolecules.

The issue regarding functional roles/partners of proteins belonging to the LSD1 family is further complicated by recently published data (*54*) which demonstrate that HsLSD1 interacts with p53 to repress p53-mediated transcriptional activation and to inhibit the role of p53 in promoting apoptosis through demethylation of residue Lys370, a residue located in the C-terminal region of p53. However, p53 C-terminal tail does not display a significant sequence homology with the histone H3 N-terminal tail (data not shown), suggesting that proteins belonging to the LSD1 family are able to recognize various substrates, most likely through differential molecular interactions.

Very recently it has been reported that in *Arabidopsis AtLSD1*/*AtLSD2* or *AtLSD3* knockout increases H3K4 methylation levels within the *FLC* and the *FWA*, whereas it does not change H3K9 and H3K27 methylation levels (*55, 56*). These data are in agreement with the specific *in vitro* demethylase activity of AtLSD1 toward H3K4 demonstrated in the present work and suggest a similar substrate specificity *in vivo*. However, in another recent report, *AtLSD1* knockout has been shown not to change the H3K4 methylation level within the *FLC* but to reduce that at H3K9 and H3K27 (*32*). The reason for such different results is not known, but it may reside in the fact that knockout of the various *AtLSDs* most probably interferes with the activity of other histone-modifying enzymes, since these have been shown to participate in multiprotein complexes in which they function in a coordinated manner (*57, 58*). This hypothesis could also explain the increase in the acetylation levels of H4 within the FLC in the *AtLSD1* and *AtLSD3* knockout *Arabidopsis* mutants (*32, 33*).

In conclusion, data presented in this paper demonstrate that AtLSD1 is a lysine-specific demethylase with a substrate specificity similar to that of HsLSD1 and an almost identical organization of the active site region. However, significant structural differences are observed at the level of the CoREST-interacting Tower domain of HsLSD1, which, together with the absence of CoREST-like proteins in the *Arabidopsis* genome, indicate that the physiological function of AtLSD1 must be dependent on the interaction with different partners from those of HsLSD1. These observations, together with the above cited report (*54*) pointing to a multifunctional role of HsLSD1 in lysine demethylation, indicate that the *in vivo* functional role of this class of proteins is a very complex one, depending on the interaction with molecular partners which may differ significantly between animal and plant lysine-specific demethylases.

ACKNOWLEDGMENT

The authors thank the *Arabidopsis* Biological Resource Centre and the DNA Stock donor for providing cDNA clone U21563, Prof. Andrea Mattevi and Dr. Claudia Binda (University of Pavia, Italy) for providing purified HsLSD1

in complex with CoREST, Dr. Alessandra Giorgi (University of Rome La Sapienza, Italy) for MALDI-TOF analyses, and Prof. Riccardo Angelini (University Roma Tre, Italy) for critical reading of the manuscript.

REFERENCES

1. Gill, G. (2004) SUMO and ubiquitin in the nucleus: different functions, similar mechanisms. *Genes Dev. 18*, 2046–2059.
2. Cohen-Armon, M., Visochek, L., Katzoff, A., Levitan, D., Susswein, A. J., Klein, R., Valbrun, M., and Schwartz, J. H. (2004) Long-term memory requires ADP-ribosylation. *Science 304*, 1820–1822.
3. Holbert, M. A., and Marmorstein, R. (2005) Structure and activity of enzymes that remove histone modifications. *Curr. Opin. Struct. Biol. 15*, 673–680.
4. Jenuwein, T., and Allis, C. D. (2001) Translating the histone code. *Science 293*, 1074–1080.
5. Forneris, F., Binda, C., Vanoni, M. A., Battaglioli, E., and Mattevi, A. (2005) Human histone demethylase LSD1 reads the histone code. *J. Biol. Chem. 280*, 41360–41365.
6. Zhang, Y., and Reinberg, D. (2001) Transcription regulation by histone methylation: interplay between different covalent modifications of the core histone tails. *Genes Dev. 15*, 2343–2360.
7. Martin, C., and Zhang, Y. (2005) The diverse functions of histone lysine methylation. *Nat. Rev. Mol. Cell Biol. 6*, 838–849.
8. Strahl, B. D., and Allis, C. D. (2000) The language of covalent histone modification. *Nature 403*, 41–45.
9. Margueron, R., Trojer, P., and Reinberg, D. (2005) The key to development: interpreting the histone code? *Curr. Opin. Genet. Dev. 15*, 163–176.
10. Sanders, S. L., Portoso, M., Mata, J., Bahler, J., Allshire, R. C., and Kouzarides, T. (2004) Methylation of histone H4 lysine 20 controls recruitment of Crb2 to sites of DNA damage. *Cell 119*, 603–614.
11. Whetstine, J. R., Nottke, A., Lan, F., Huarte, M., Smolikov, S., Chen, Z., Spooner, E., Li, E., Zhang, G., Colaiacovo, M., and Shi, Y. (2006) Reversal of histone lysine trimethylation by the JMJD2 family of histone demethylases. *Cell 125*, 467–481.
12. Kouzarides, T. (2002) Histone methylation in transcriptional control. *Curr. Opin. Genet. Dev. 12*, 198–209.
13. Cuthbert, G. L., Daujat, S., Snowden, A. W., Erdjument-Bromage, H., Hagiwara, T., Yamada, M., Schneider, R., Gregory, P. D., Tempst, P., Bannister, A. J., and Kouzarides, T. (2004) Histone deimination antagonizes arginine methylation. *Cell 118*, 545–553.
14. Wang, Y., Wysocka, J., Sayegh, J., Lee, Y. H., Perlin, J. R., Leonelli, L., Sonbuchner, L. S., McDonald, C. H., Cook, R. G., Dou, Y., Roeder, R. G., Clarke, S., Stallcup, M. R., Allis, C. D., and Coonrod, S. A. (2004) Human PAD4 regulates histone arginine methylation levels via demethylimination. *Science 306*, 279–283.
15. Shi, Y., Lan, F., Matson, C., Mulligan, P., Whetstine, J. R., Cole, P. A., Casero, R. A., and Shi, Y. (2004) Histone demethylation mediated by the nuclear amine oxidase homolog LSD1. *Cell 119*, 941–953.
16. Tsukada, Y., Fang, J., Erdjument-Bromage, H., Warren, M. E., Borchers, C. H., Tempst, P., and Zhang, Y. (2006) Histone demethylation by a family of JmjC domain-containing proteins. *Nature 439*, 811–816.
17. Yamane, K., Toumazou, C., Tsukada, Y., Erdjument-Bromage, H., Tempst, P., Wong, J., and Zhang, Y. (2006) JHDM2A, a JmjC-containing H3K9 demethylase, facilitates transcription activation by androgen receptor. *Cell 125*, 483–495.
18. Humphrey, G. W., Wang, Y., Russanova, V. R., Hirai, T., Qin, J., Nakatani, Y., and Howard, B. H. (2001) Stable histone deacetylase complexes distinguished by the presence of SANT domain proteins CoREST/kiaa0071 and Mta-L1. *J. Biol. Chem. 276*, 6817–6824.
19. Lee, M. G., Wynder, C., Cooch, N., and Shiekhattar, R. (2005) An essential role for CoREST in nucleosomal histone 3 lysine 4 demethylation. *Nature 437*, 432–435.
20. Shi, Y. J., Matson, C., Lan, F., Iwase, S., Baba, T., and Shi, Y. (2005) Regulation of LSD1 histone demethylase activity by its associated factors. *Mol. Cell 19*, 857–864.
21. Metzger, E., Wissmann, M., Yin, N., Müller, J. M., Schneider, R., Peters, A. H., Günther, T., Buettner, R., and Schüle, R. (2005) LSD1 demethylates repressive histone marks to promote androgen-receptor-dependent transcription. *Nature 437*, 436–439.
22. Stavropoulos, P., Blobel, G., and Hoelz, A. (2006) Crystal structure and mechanism of human lysine-specific demethylase-1. *Nat. Struct. Mol. Biol. 13*, 626–632.
23. Chen, Y., Yang, Y., Wang, F., Wan, K., Yamane, K., Zhang, Y., and Lei, M. (2006) Crystal structure of human histone lysine-specific demethylase 1 (LSD1). *Proc. Natl. Acad. Sci. U.S.A. 103*, 13956–13961.
24. Yang, M., Gocke, C. B., Luo, X., Borek, D., Tomchick, D. R., Machius, M., Otwinowski, Z., and Yu, H. (2006) Structural basis for CoREST-dependent demethylation of nucleosomes by the human LSD1 histone demethylase. *Mol. Cell 23*, 377–387.
25. Yang, M., Cullane, J. C., Szewczuk, L. M., Gocke, C. B., Brautigam, C. A., Tomchick, D. R., Machius, M., Cole, P. A., and Yu, H. (2007) Structural basis of histone demethylation by LSD1 revealed by suicide inactivation. *Nat. Struct. Mol. Biol. 14*, 535–539.
26. Forneris, F., Binda, C., Adamo, A., Battaglioli, E., and Mattevi, A. (2007) Structural basis of LSD1-CoREST selectivity in histone H3 recognition. *J. Biol. Chem. 282*, 20070–20074.
27. Yang, M., Cullane, J. C., Szewczuk, L. M., Jalili, P., Ball, H. L., Machius, M., Cole, P. A., and Yu, H. (2007) Structural basis for the inhibition of the LSD1 histone demethylase by the antidepressant *trans*-2-phenylcyclopropylamine. *Biochemistry 46*, 8058–8065.
28. Forneris, F., Binda, C., Dall'Aglio, A., Fraaije, M. W., Battaglioli, E., and Mattevi, A. (2006) A highly specific mechanism of histone H3-K4 recognition by histone demethylase LSD1. *J. Biol. Chem. 281*, 35289–35295.
29. Jasencakova, Z., Soppe, W. J., Meister, A., Gernand, D., Turner, B. M., and Schubert, I. (2003) Histone modifications in *Arabidopsis*—high methylation of H3 lysine 9 is dispensable for constitutive heterochromatin. *Plant J. 33*, 471–480.
30. Lippman, Z., Gendrel, A. V., Black, M., Vaughn, M. W., Dedhia, N., McCombie, W. R., Lavine, K., Mittal, V., May, B., Kasschau, K. D., Carrington, J. C., Doerge, R. W., Colot, V., and Martienssen, R. (2004) Role of transposable elements in heterochromatin and epigenetic control. *Nature 430*, 471–476.
31. Bastow, R., Mylne, J. S., Lister, C., Lippman, Z., Martienssen, R. A., and Dean, C. (2004) Vernalization requires epigenetic silencing of FLC by histone methylation. *Nature 427*, 164–167.
32. Krichevsky, A., Gutgarts, H., Kozlovsky, S. V., Tzfira, T., Sutton, A., Sternglanz, R., Mandel, G., and Citovsky, V. (2007) C2H2 zinc finger-SET histone methyltransferase is a plant-specific chromatin modifier. *Dev. Biol. 303*, 259–269.
33. He, Y., Michaels, S. D., and Amasino, R. M. (2003) Regulation of flowering time by histone acetylation in *Arabidopsis*. *Science 302*, 1751–1754.
34. Altschul, S. F., Madden, T. L., Schaffer, A. A., Zhang, J., Zhang, Z., Miller, W., and Lipman, D. J. (1997) Gapped BLAST and PSI-BLAST: a new generation of protein database search programs. *Nucleic Acids Res. 25*, 3389–3402.
35. Thompson, J. D., Higgins, D. G., and Gibson, T. J. (1994) CLUSTAL W: improving the sensitivity of progressive multiple sequence alignment through sequence weighting, position-specific gap penalties and weight matrix choice. *Nucleic Acids Res. 22*, 4673–4680.
36. Forneris, F., Binda, C., Vanoni, M. A., Mattevi, A., and Battaglioli, E. (2005) Histone demethylation catalysed by LSD1 is a flavin-dependent oxidative process. *FEBS Lett. 579*, 2203–2207.
37. Deleage, G., and Geourjon, C. (1993) An interactive graphic program for calculating the secondary structure content of proteins from circular dichroism spectrum. *Comput. Appl. Biosci. 2*, 197–199.
38. Holt, A., and Baker, G. B. (1995) Metabolism of agmatine (clonidine-displacing substance) by diamine oxidase and the possible implications for studies of imidazoline receptors. *Prog. Brain Res. 106*, 187–197.
39. Laemmli, U. K. (1970) Cleavage of structural proteins during the assembly of the head of bacteriophage T4. *Nature 277*, 680–685.
40. Gehrig, H. H., Winter, K., Cushman, J., Borland, A., and Taybi, T. (2000) An improved RNA isolation method for succulent plant species rich in polyphenols and polysaccharides. *Plant Mol. Biol. Rep. 18*, 369–376.
41. Petrey, D., Xiang, Z., Tang, C. L., Xie, L., Gimpelev, M., Mitros, T., Soto, C. S., Goldsmith-Fischman, S., Kernytsky, A., Schlessinger, A., Koh, I. Y., Alexov, E., and Honig, B. (2003) Using multiple structure alignments, fast model building, and energetic analysis in fold recognition and homology modeling. *Proteins 53*, 430–435.

42. Laskowski, R. A., MacArthur, M. W., Moss, D. S., and Thornton, J. M. (1993) PROCHECK: a program to check the stereochemical quality of protein structures. *J. Appl. Crystallogr. 26*, 283–291.
43. Rocchia, W., Alexov, E., and Honig, B. (2001) Extending the applicability of the nonlinear Poisson-Boltzmann equation: Multiple dielectric constants and multivalent ions. *J. Phys. Chem. B 105*, 6507–6514.
44. Pettersen, E. F., Goddard, T. D., Huang, C. C., Couch, G. S., Greenblatt, D. M., Meng, E. C., and Ferrin, T. E. (2004) UCSF chimera—A visualization system for exploratory research and analysis. *J. Comput. Chem. 25*, 1605–1612.
45. Brooks, B. R., Bruccoleri, R. E., Olafson, B. D., States, D. J., Swaminathan, S., and Karplus, M. (1983) CHARMM: A Program for Macromolecular Energy, Minimization, and Dynamics Calculations. *J. Comput. Chem. 4*, 187–217.
46. MacKerell, A. D., Jr., Bashford, D., Bellott, M., Jr., Evanseck, J. D., Field, M. J., Fischer, S., Gao, J., Guo, H., Ha, S., Joseph-McCarthy, D., Kuchnir, L., Kuczera, K., Lau, F. T. K., Mattos, C., Michnick, S., Ngo, T., Nguyen, D. T., Prodhom, B., Reiher, W. E., III, Roux, B., Schlenkrich, M., Smith, J. C., Stote, R., Straub, J., Watanabe, M., Wiorkiewicz-Kuczera, J., Yin, D., and Karplus, M. (1998) All-atom empirical potential for molecular modeling and dynamics studies of proteins. *J. Phys. Chem. B 102*, 3586–3616.
47. Tavladoraki, P., Rossi, M. N., Saccuti, G., Perez-Amador, M. A., Polticelli, F., Angelini, R., and Federico, R. (2006) Heterologous expression and biochemical characterization of a polyamine oxidase from *Arabidopsis thaliana* involved in polyamine back-conversion. *Plant Physiol. 141*, 1519–1532.
48. Nicolas, E., Lee, M. G., Hakimi, M. A., Cam, H. P., Grewal, S. I., and Shiekhattar, R. (2006) Fission yeast homologs of human histone H3 lysine 4 demethylase regulate a common set of genes with diverse functions. *J. Biol. Chem. 281*, 35983–35988.
49. Bradley, C., van der Meer, R., Roodi, N., Yan, H., Chandrasekharan, M. B., Sun, Z. W., Mernaugh, R. L., and Parl, F. F. (2007) Carcinogen-induced histone alteration in normal human mammary epithelial cells. *Carcinogenesis 28*, 2184–2192.
50. He, Y., and Amasino, R. M. (2005) Role of chromatin modification in flowering-time control. *Trends Plant Sci. 10*, 30–35.
51. Provencher, S. W. (1982) A constrained regularization method for inverting data represented by linear algebraic or integral-equations. *Comput. Phys. Commun. 27*, 213–227.
52. Andrade, M. A., Chacon, P., Merelo, J. J., and Moran, F. (1993) Evaluation of secondary structure of proteins from UV circular dichroism spectra using an unsupervised learning neural network. *Protein Eng. 6*, 383–390.
53. Sreerama, N., Venyaminov, S. Y., and Woody, R. W. (1999) Estimation of the number of alpha-helical and beta-strand segments in proteins using circular dichroism spectroscopy. *Protein Sci. 8*, 370–380.
54. Huang, J., Sengupta, R., Espejo, A. B., Lee, M. G., Dorsey, J. A., Richter, M., Opravil, S., Shiekhattar, R., Bedford, M. T., Jenuwein, T., and Berger, S. L. (2007) p53 is regulated by the lysine demethylase LSD1. *Nature 449*, 105–108.
55. Jiang, D., Yang, W., He, Y., and Amasino, R. M. (2007) *Arabidopsis* relatives of the human lysine-specific demethylase 1 repress the expression of FWA and FLOWERING LOCUS C and thus promote the floral transition. *Plant Cell 19*, 2975–2987.
56. Liu, F., Quesada, V., Crevillén, P., Bäurle, I., Swiezewski, S., and Dean, C. (2007) The *Arabidopsis* RNA-binding protein FCA requires a lysine-specific demethylase 1 homolog to downregulate FLC. *Mol. Cell 28*, 398–407.
57. Lee, M. G., Wynder, C., Bochar, D. A., Hakimi, M. A., Cooch, N., and Shiekhattar, R. (2006) Functional interplay between histone demethylase and deacetylase enzymes. *Mol. Cell. Biol. 26*, 6395–6402.
58. Wissmann, M., Yin, N., Müller, J. M., Greschik, H., Fodor, B. D., Jenuwein, T., Vogler, C., Schneider, R., Günther, T., Buettner, R., Metzger, E., and Schüle, R. (2007) Cooperative demethylation by JMJD2C and LSD1 promotes androgen receptor-dependent gene expression. *Nat. Cell Biol. 9*, 347–353.

BI701969K